Optimization of a Hybrid Backward Bent Duct Buoy with Point Absorber Based on Kuantan Harbor Ocean Characteristics

Muhamad Aiman Jalani[1], Mohd Rashdan Saad[1], Mohd Azzeri Md Naiem[2], Noh Zainal Abidin[2], Mohd Norsyarizad Razali[2], Yasutaka Imai[3], Muhammad Harith Halim[4], Muhamad Syahmi Sulaiman[5], Mohd Rosdzimin Abdul Rahman[1]

Wave energy is attractive due to its generosity, sustainability and cleanliness. A combination of an Oscillating Water Column (OWC) and Oscillating Buoy (OB) is an economical approach to harness wave energy. In this work, a hybrid system constising of Backward Bent Duct Buoy (BBDB) and a floating Point Absorber (PA) was investigated. The PA is attached to the front of the BBDB system. The two devices are aligned in the direction of the incident wave, with the PA deployed upstream of the BBDB. The experiment was conducted based on data collected during the northeast monsoon, southwest monsoon, and transition period regarding sea characteristics in a near-shore region of Kuantan harbor. The hybrid BBDB-PA was scaled up to a laboratory scale by Froude scaling to support physical conditions similar to those at specific ocean sites. A series of physical experiments were conducted in a 2D wave flume to understand the effects of wave period and slit length of the hybrid wave energy converter (WEC) system. Compared to the individual devices of BBDB and PA, the hybrid system design provides a higher peak response amplitude operator (RAO) as well as better performance. In addition, the gap length between PA and BBDB was directly correlated to a wavelength corresponding to the theoretical value for the peak-to-trough length at which the maximum wave height occurs. Regardless of the different geometries of the hybrid wind turbines, it was found that the resonant frequency contributes to optimal performance regardless of the characteristics of the hybrid wind turbines. This research recommends the optimization of power generation from the sea to maximize the space in the sea for power generation.

KEYWORDS
~ Wave energy
~ Hydrodynamics
~ BBDB
~ Point ABsorber
~ Hybrid WEC
~ Optimization

[1] Universiti Pertahanan Nasional Malaysia, Faculty of Engineering, Kuala Lumpur, Malaysia
[2] Universiti Pertahanan Nasional Malaysia, Faculty of Defence Science and Technology, Kuala Lumpur, Malaysia
[3] Institute of Ocean Energy, Saga University, Japan
[4] Kuantan Port Consortium, Kuantan, Pahang, Malaysia
[5] Kuantan Port Authority, Operation and Regulatory Division, Kuantan, Pahang, Malaysia
e-mail: rosdzimin@gmail.com
doi: 10.7225/toms.v14.n01.006

Received: 23 Jan 2024 / Revised: 23 Dec 2024 / Accepted: 7 Feb 2025 / Published: 20 Apr 2025

1. INTRODUCTION

In contemporary times, the phenomenon of urbanization and the simultaneous increase in the world's population have had a significant impact on energy consumption on a global scale. The use of energy infrastructures that rely on fossil fuels is associated with various adverse consequences for the environment. These include the emission of air pollutants, the exacerbation of global warming through the release of carbon dioxide (CO_2) and other greenhouse gasses, the creation of acid rain, the depletion of finite energy resources and the deterioration of environmental conditions. Furthermore, climate change can be considered as a consequence of global warming (Amin et al., 2022). Furthermore, dependence on fossil fuels leads to diminishing fossil fuel reserves and contributes to the problem of energy security (Shadman et al., 2021). Renewable energies are widely recognized as carbon-free energy sources that have the potential to effectively solve the problem of energy security and reduce the release of CO_2 into the atmosphere (Raihan and Tuspekova, 2022). The COVID-19 pandemic in 2020 has drastically changed the global demand for energy. According to the International Energy Agency (IEA), demand for oil (9%), coal (8%), natural gas (5%) and nuclear energy (2%) will decrease from 2020, while demand for renewable energy could increase by 1% (Chowdhury et al., 2021). To contribute to such improvements, renewable energy must be used on a large scale. However, the utilization of such resources requires extensive improvements in energy conversion and distribution systems. Therefore, the focus of this study was on ocean energy and wave energy due to their advantageous characteristics. It is worth noting that special attention was given to wave energy, one of the densest, most predictable and consistent energy sources (Lavidas and Blok, 2021). Malaysia is one of the countries with significant potential for harnessing ocean energy for power generation as it has a 4,675 km coastline along the South China Sea and the Strait of Malacca (Kai et al., 2021). Malaysia also has strong seasonal monsoon winds that cause the country to always have turbulent waves in the sea and in some areas (Isa et al., 2021). Assuming that the geographical advantage of Malaysia being surrounded by the sea can be properly utilized. In this case, the development and exploration of ocean utilization would go a long way in solving the problems of difficult energy consumption in Malaysia. Kuantan Port is a privatized port on the east coast of Malaysia's Pahang Peninsula with access to the South China Sea. Geographically, the port serves the shortest shipping route between Malaysia and China and is only 45 minutes by air from Kuala Lumpur. Alternatively, Kuala Lumpur can be reached via the Kuala Lumpur-Karak Expressway in three hours. In addition, Kuantan Port has a 4.63 km breakwater which offers advantages for the installation of Wave Energy Converters (WEC) due to the cost savings on subsea cables. In addition, most previous studies have mentioned the advantage of integrating WECs with breakwaters. Zhao et al. mention in their studies that the integration of WECs with breakwaters not only reduces the high construction cost but also can improve the energy harvesting performance of WECs (Zhao et al., 2021). In addition, Zhao et al. found in their study that placing WEC in front of a breakwater generates a larger heave Response Amplitude Operator (RAO) and greater wave power (Zhao et al., 2019).

Oscillating Water Column (OWC), Oscillating Buoy (OB) and Over Topping (OT) are examples of WECs based on different operating principles (Zhang et al., 2021), with OWC and OB receiving more attention due to their geometric simplicity. In recent years, most researchers have started to look for better ways to utilize ocean energy. This has opened up a good opportunity to explore and create a new hybrid or multi-platform system. All the energy from the ocean is utilized by systems that allow other resources to be used at the same location in the ocean. Experiments and modeling have been used to learn more about the hybrid or multiplatform structure of the WEC system. The main goal of hybrid energy system research is to improve the efficiency of the combined system in power generation and optimize its design. In the recent study conducted by Wan et al., the integration of a WEC with floating body into a hybrid OWC system with breakwater is investigated (Wan et al., 2023). Using Star-CCM and computational fluid dynamics (CFD) tools, they conduct a numerical study on the hydrodynamic performance of the hybrid system. The bottoms of four different types of floats are compared and analyzed. They found that the hybrid system with the Berkley wedge bottom shape can achieve a CWR value of up to 81.2%, which is due to the improved wave damping of the asymmetric floats. In addition, Yang et al. combined a WEC with wave floats with an OWC and investigated the hydrodynamic performance of the hybrid system with a numerical wave tank (Yang et al., 2023). They found that the combination of floats and breakwater WTs significantly improved the frequency bandwidth, resulting in an increase in efficiency to 83.28%. In comparison, the efficiency of a single device was only 57%. In addition, Cheng et al. (2022) investigated the combination of an OWC and an OB to develop a hybrid WEC system that serves as a floating breakwater (Cheng et al., 2022). In terms of wave energy conversion, they found that the OB outperformed the OWC. The resonance between the OWC and the OB has a negative impact on the extraction of wave energy, while its effect on wave attenuation is considered insignificant. In the long-period wave regime, it was found that the OWC system, which is characterized by a deeper intake and a symmetrical wall configuration, shows better results in both wave energy extraction and wave attenuation. However, there is still a lack of analysis on the interaction between two different floating WEC bodies, especially between OWC and OB. The addition of PA to the BBDB body will have different effects and vibrations on both devices, so a systematic study is needed in this area. The possibility of synergies for this concept has been numerically investigated by Jalani et al. (2023). They investigate the effects of using a novel hybrid Backward Bent Duct Buoy (BBDB) with a Point Absorber (PA) under different wave conditions. They show that the new hybrid shape significantly affects the additional mass, the radiation attenuation coefficient and the excitation force of the

BBDB and the PA. In addition, the parameter optimization of the integration of the hybrid BBDB with the PA has a positive effect on the wave attenuation and thus contributes to a better performance.

Based on previous research, it is clear that hybrid WECs can improve performance by combining the benefits of each WEC. BBDB is known to be very sensitive to wave direction (Portillo et al., 2019), which is not the case with PA. The utilization of a hybrid system with PA can effectively mitigate the sensitivity of BBDB to wave direction. Consequently, the combination of PA and BBDB has the potential to improve the efficiency of wave energy harvesting regardless of wave direction. Furthermore, the properties and performance of a hybrid of BBDB and PA have not yet been experimentally explored in the existing literature. Therefore, based on previous research on BBDB and PA technology, it is believed that the optimization of WEC parameters can significantly contribute to the oscillatory motion of the WEC device and ultimately affect the performance. It was also found that the effects of hybrid BBDB-PA integration on performance still needs to be investigated. Therefore, this study was conducted to investigate the characteristics and performance of hybrid BBDB-PA integration with different state parameters and wave conditions. Since the hybrid WEC technique has many advantages, this paper attempts to investigate the characteristics and performance of hybrid BBDB-PA.

The following sections of this paper are organized as follows: Section 2 contains an analysis of the data collection and simulation in relation to the site characteristics (specifically water depth, wave height and wave period) in which the hybrid WEC was deployed. The design of the experiment, i.e. the tank setup, sensor device, calibration and fabrication are presented in Section 3. The data analysis to obtain the results of the experiment is presented in Section 4. Section 5 illustrates the results and discussion for the comparative analysis of hybrid and non-hybrid results, comparing the experimental model with the Heave RAO. The conclusions are summarized in Section 6.

2. LOCATION AND CHARACTERISTICS OF THE SEA

The objectives of this study were first specified on the basis of the literature analysis. The objectives of the study were chosen to investigate the characteristics of a hybrid WEC by applying a new form of hybrid BBDB and PA. This research selected dimensions and conditions based on previous studies to validate and investigate the primary performance by integrating the hybrid form WEC. The next task of this research is to select the condition parameters (factors) to optimise the optimal values and develop an empirical model of a hybrid BBDB with PA based on the wave conditions at the site. Kuantan harbor was selected as the site for this research as this site has many advantages for the installation of wind turbines in terms of economic and environmental aspects and also shows the behaviour of Malaysian marine conditions.

The data in Kuantan Harbour was collected over a period of one week using the Acoustic Wave and Current (AWAC) Profiler and validated using Delft3D numerical software from the Institute of Oceanography and Environment, Universiti Malaysia Terengganu (UMT). The wave data was projected for the period of the northeast monsoon (December 6 to 15, 2019), the southwest monsoon (July 6 to 15, 2020) and the transition period (October 6 to 15, 2020). The exact location of the WEC is in Tanjung Gelang in the eastern part of Peninsular Malaysia between 03˚ 58’ north latitude and 103˚ 26.4’ east longitude. This port is located 25 km from the city centre of Kuantan in Pahang. The port of Kuantan is currently developing rapidly into a major international port, which has led to an increase in the number of manufacturing and industrial operations. Overlooking the South China Sea, this port serves as an important sea route to major ports in the Asia-Pacific region.

The bathymetry of the Kuantan Harbor simulation area varies between 0 and 16 m water depth (Figure 1). The water depths are generally deeper within the port area and slightly shallower in the nearshore area.

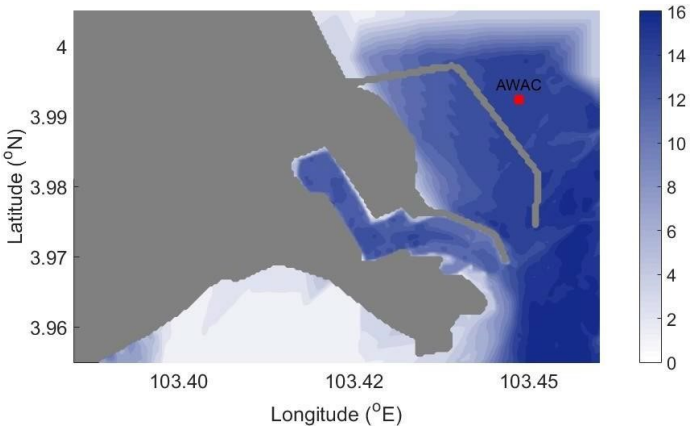

Figure 1. The bathymetry of Kuantan harbor. The red dot indicates the location of the acoustic wave and current profiler (AWAC) profiler.

Figure 2 illustrates the temporal variation of the significant wave height during the simulation period. The significant wave height was highest during the northeast monsoon at 0.78 – 1.30 m (Figure 2 and Table 1). Meanwhile, the significant wave heights during the southwest monsoon and the transition period were almost identical and had a similar average value of 0.8 m (Figure 2 and Table 1). As for the wave period in Kuantan harbor, the northeast monsoon recorded the shortest wave period in the range of 2.8 – 3.6 s (Figure 3). In contrast, during the southwest monsoon and the transition period, the wave period was between 3 and 6 s (Figure 3).

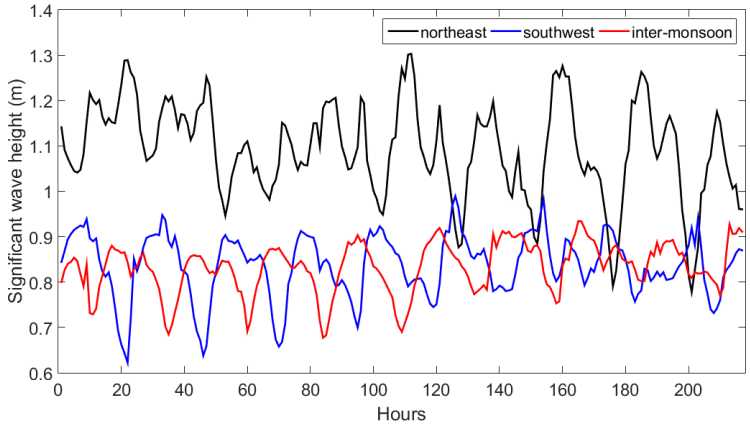

Figure 2. Significant wave height during the simulation period.

	Northeast monsoon	Southwest monsoon	Inter-monsoon
Minimum	0.78	0.62	0.68
Maximum	1.30	0.99	0.94
Average	1.09	0.84	0.83

Table 1. Minimum, maximum and average of the significant wave height. The unit of measurement is m.

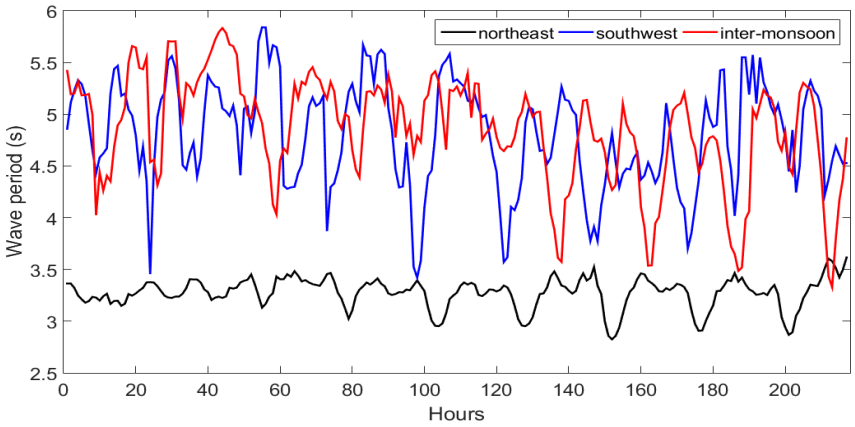

Figure 3. Wave during the simulation period.

Regarding the wave patterns in Kuantan harbor during the different monsoon seasons, it was found that the northeast monsoon was characterized by the largest wave height, followed by the southwest monsoon and the intermediate monsoon (Figure 4a). During the northeast monsoon, strong waves with a maximum intensity of 1.5 m/s propagated from the coastal area towards the coast (Figure 4a). However, it was immediately reduced when it reached the breakwater (Figure 4a). Similar trends were also observed during the southwest monsoon and the intermediate monsoon, where the wave propagated towards the coast and its energy was reduced when it reached the breakwater (Figures 4b and 4c).

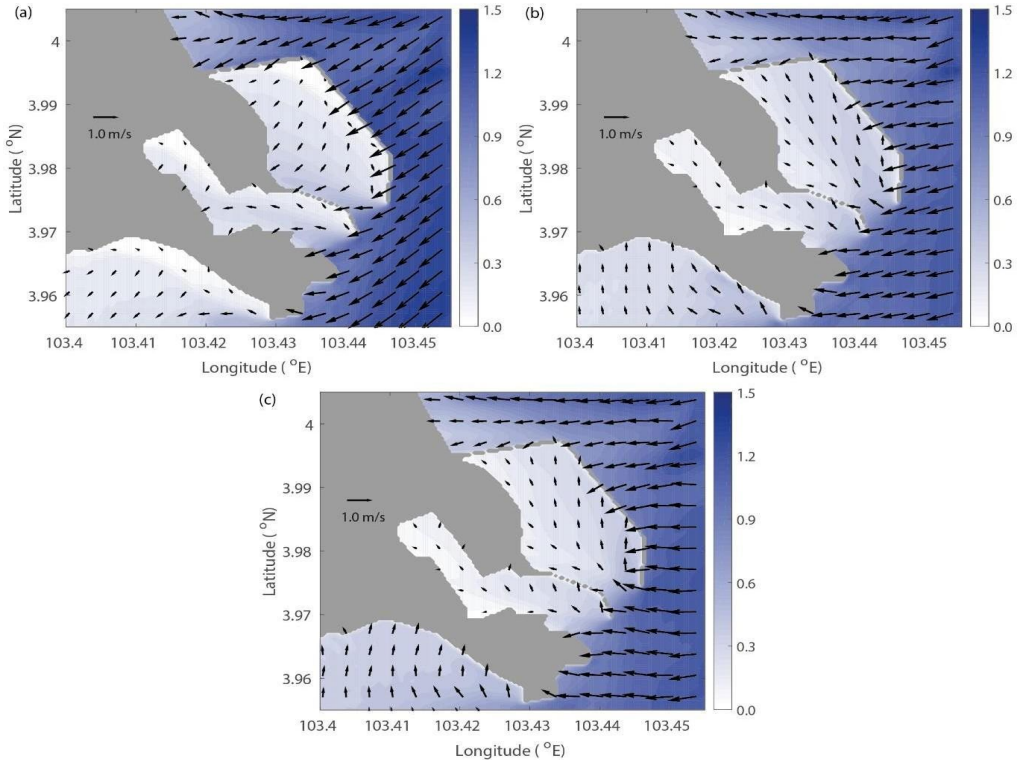

Figure 4. The wave pattern of Kuantan Port during the (a) northeast monsoon, (b) southwest monsoon, and (c) inter-monsoon. The unit of measurement is m.

3. EXPERIMENTAL SETUP

The experiments were conducted in the wave flume at Universiti Pertahanan Nasional Malaysia (UPNM) (see Figure 5). The flume was 7 m long, 2 m wide and 1.5 m deep. The wave flume was equipped with an absorbing wave maker of a highly repeatable type. This wave maker ensures that the generated wave remains the same during a single trial by absorbing the reflected and radiated wave generated by the device. At the other end of the basin, a beach with a high-quality variable slope was created to absorb the wave and prevent reflection from the test objects, whose reflection coefficient is normally less than 5%. The water depth was 1.25 m. In this study, the range of wave height and wave period is 0.05 - 0.15 m and 1 - 5 s, respectively. The range was chosen due to the suitability of the waves for low wave height conditions.

Figure 5. 2D wave flume at UPNM.

In order to better compare the designs from the previous section, the hybrid BBDB-PA was scaled down to laboratory scale to create similar physical conditions for the wave characteristics in Kuantan Harbour to ensure similarity. The geometric, kinematic and dynamic similarities between the laboratory model and its real scale must be met to achieve

a match between the two. Several theories of scale similarity have been presented and established for studying the responses of common offshore structures (Hughes, 1993; Chakrabarti, 1999), which can be useful for determining dimensionless numbers such as Froude (Fr), Reynolds (Re), Mach (Mn), Weber (Wn), Keulegan-Carpenter (KC) and Strouhall (St). These dimensionless numbers stand for the force ratios inertia/gravity (Fr), inertia/viscosity (Re), inertia/elasticity (Mn), inertia/surface tension (Wn), drag/inertia (KC) and the dimensionless vortex shedding frequency (St), respectively (Giannini et al., 2020). The first two numbers are the most common and important dimensionless values for this investigation to achieve full hydrodynamic similarity (Froude & Reynolds). However, as stated by Celik and Altunkaynak (2019), it is almost impossible to maintain the same Fr and Re number between the model scale and the original size (Celik and Altunkaynak, 2019). Therefore, the similarity of Re was ignored in this work, while the stability of Fr number was considered for model and prototype scales.

Maintaining a relatively constant Fr number with respect to the real-scale prototype and model-scale version should be a priority. The Fr similarity criteria, also known as gravity similarity criteria, are widely regarded as the primary similarity criteria in physical modelling experiments on fluid-structure interaction of floating structures. The main objective is to ensure that the gravitational force on the structure remains the same for the prototype and the scale model. For the Fr analogy to be fulfilled, the Fr number should be the same in the prototype and the scaled model. In order to scale a WEC appropriately, a specific compromise must therefore be developed. The Fr number, Fr, is defined as (Qiao et al., 2021):

$$Fr = \frac{F_{inertia}}{G} = \frac{\rho L^2 v^2}{\rho L^3 g} = \frac{v}{\sqrt{gL}}, \quad (1)$$

where $F_{inertia}$ stands for the force of inertia, G for the force of gravity, ρ for the density of the fluid, v for the characteristic velocity of the fluid, v, L for the characteristic length of the device and, and g for the acceleration due to gravity. The Fr number indicates the relative importance of the inertial forces and gravity. As this is an approximation process, the results are not without error. For this study, the 1:30 scaling ratio was applied based on the Fr number calculation for the prototype and the scaled model, taking into account the experimental limitations.

The calibration of the instruments was first performed to determine the transfer function that would match the measured physical quantities with the signal generated by the instruments. This allows the signal data to be converted directly into the measured physical values. Figure 6 shows an ultrasonic level sensor that continuously transmits high-frequency sound waves to a target object, in this case the water surface. It measures the time that elapses between the emission of the sound waves and the detection of their echo. Therefore, the speed of sound was used to determine the distance between the sensor and the target object. However, the update frequency of the ultrasonic waves was relatively low, usually below 100 Hz. In addition, the ultrasonic level sensor cannot measure steep waves because the sound is not reflected to the receiver when the wave slope is high. For this experiment, the KEYENCE FW-H07 ultrasonic level sensor (±0.001 m accuracy) was selected to measure the water level in a floating OWC chamber.

Figure 6. Ultrasonic level sensor

Despite the manufacturer calibrated the ultrasonic measurement device, it was recalibrated to quantify the uncertainty. As depicted in Figure 7, the ultrasonic level sensor was calibrated by attaching it to a horizontally scaled calibration block and moving the sensor backwards to obtain different immersion depths (distances). It is recommended to calibrate the wave probes in ten equal increments to obtain an accurate transfer function and a better calculation of the uncertainty. The calibration range consists of the largest possible range of the measurement (ITTC, 2017). However, in the current test, this criterion was not met as the maximum range of the calibration plate was limited to 100 mm. It is advisable to collect at least 100 samples at each data point during the calibration process to minimize the uncertainty resulting from

the selection of different data ranges. The ultrasonic level results from the calibration of the ultrasonic level sensor are shown in Figure 8. The value equation from the graph was multiplied by the sensor value to obtain the actual value.

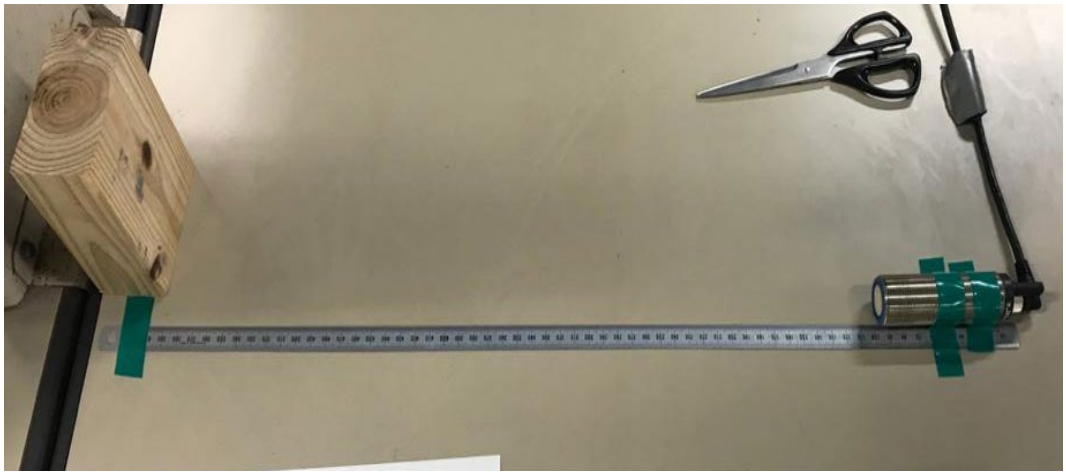

Figure 7. Ultrasonic liquid level sensor calibration.

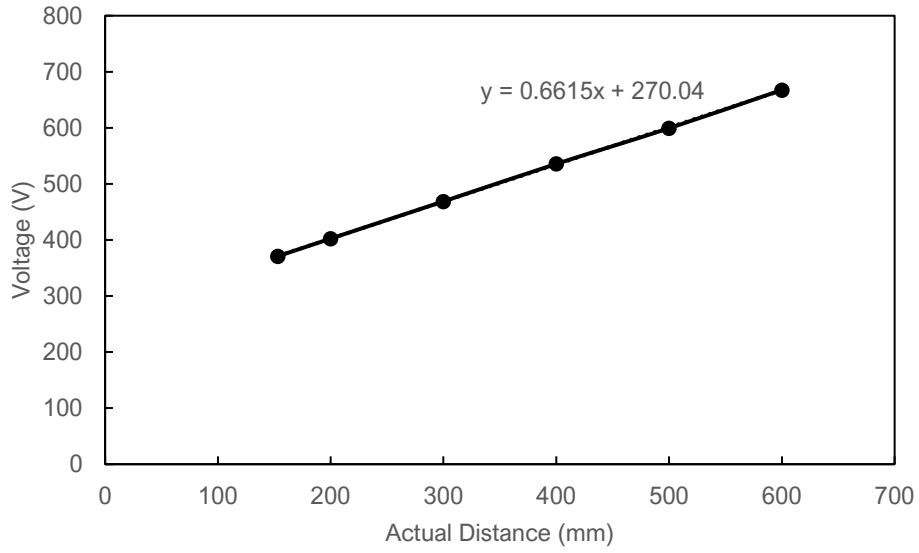

Figure 8. Ultrasonic sensor calibration result.

To ensure the accuracy and precision of the experiment, the locations in the 2D wave tank where the correct wave conditions prevail must be determined. The wave tank was divided into five different locations where the sensor should be placed. The center of the working length was chosen as the middle location (location 3). Locations 1, 2, 4 and 5 were determined every 30 cm to the left and right of this. These locations provided sufficient distance to prevent interference of the evanescent wave by the wave generator and at the same time allow sufficient time for the incident wave to be evaluated before the radiated wave reflected by the wave absorber overlaps with the incident wave. Each location has a distance of 0.30 m from the others, as this was favorable for mounting the sensor, as shown in Figure 9. Each location was tested with three different wave heights, namely 0.04 m, 0.08 m and 0.12 m. A set of aluminum frames was used to mount the sensor at the same distance above the water surface, as shown in Figure 10. The sensor was mounted 0.75 m above the water surface for each location. The software was then connected to the sensor to record the wave height movement. Due to the specifications of the sensor, only the wave height movements were recorded for this study.

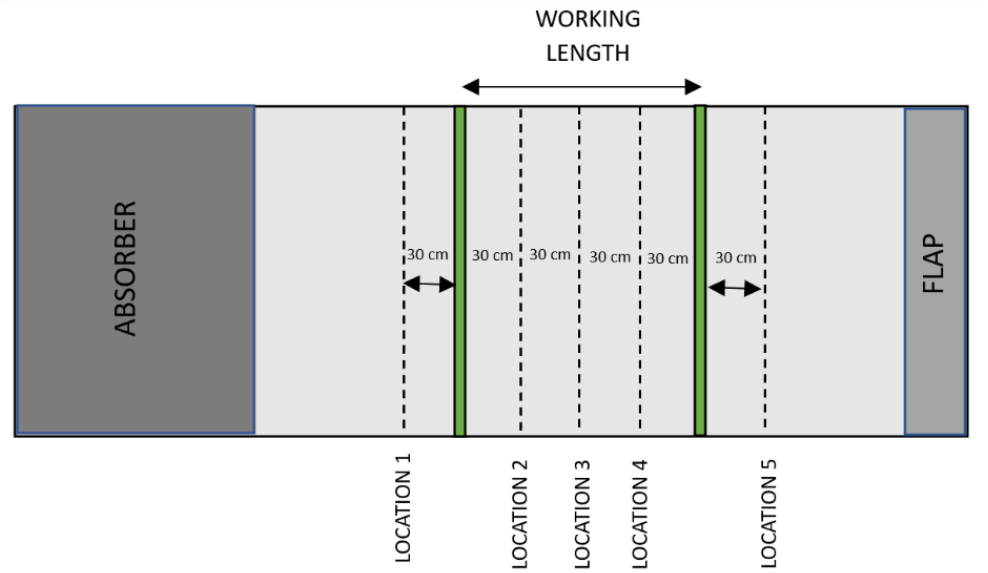

Figure 9. Location for wave data calibration.

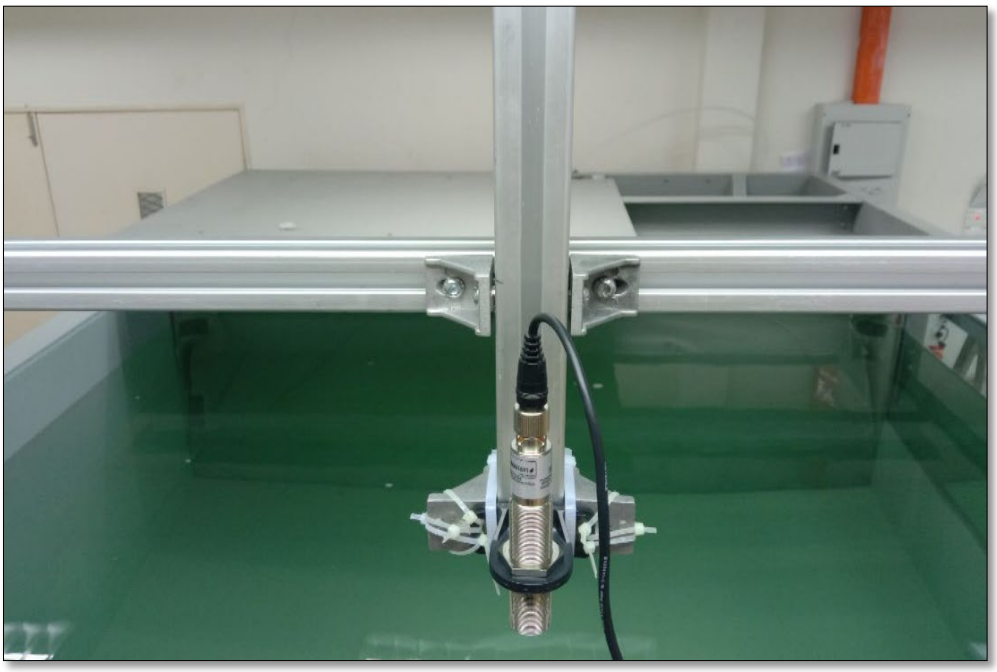

Figure 10. Ultrasonic sensor mounted on Aluminum Frame

The data collected during the experiment was the wave height measured by the sensor in a range of 20 s for each test compared to the time series. The average difference in wave height was then calculated and taken as the measured data and compared to the input data to generate an R-squared (coefficient of determination). The value of R-squared can vary between 0 and 1. R-squared is usually described as a measure of the ability of the regression model to explain the data. A larger R-squared value indicates that the model covers a larger part of the large variability.

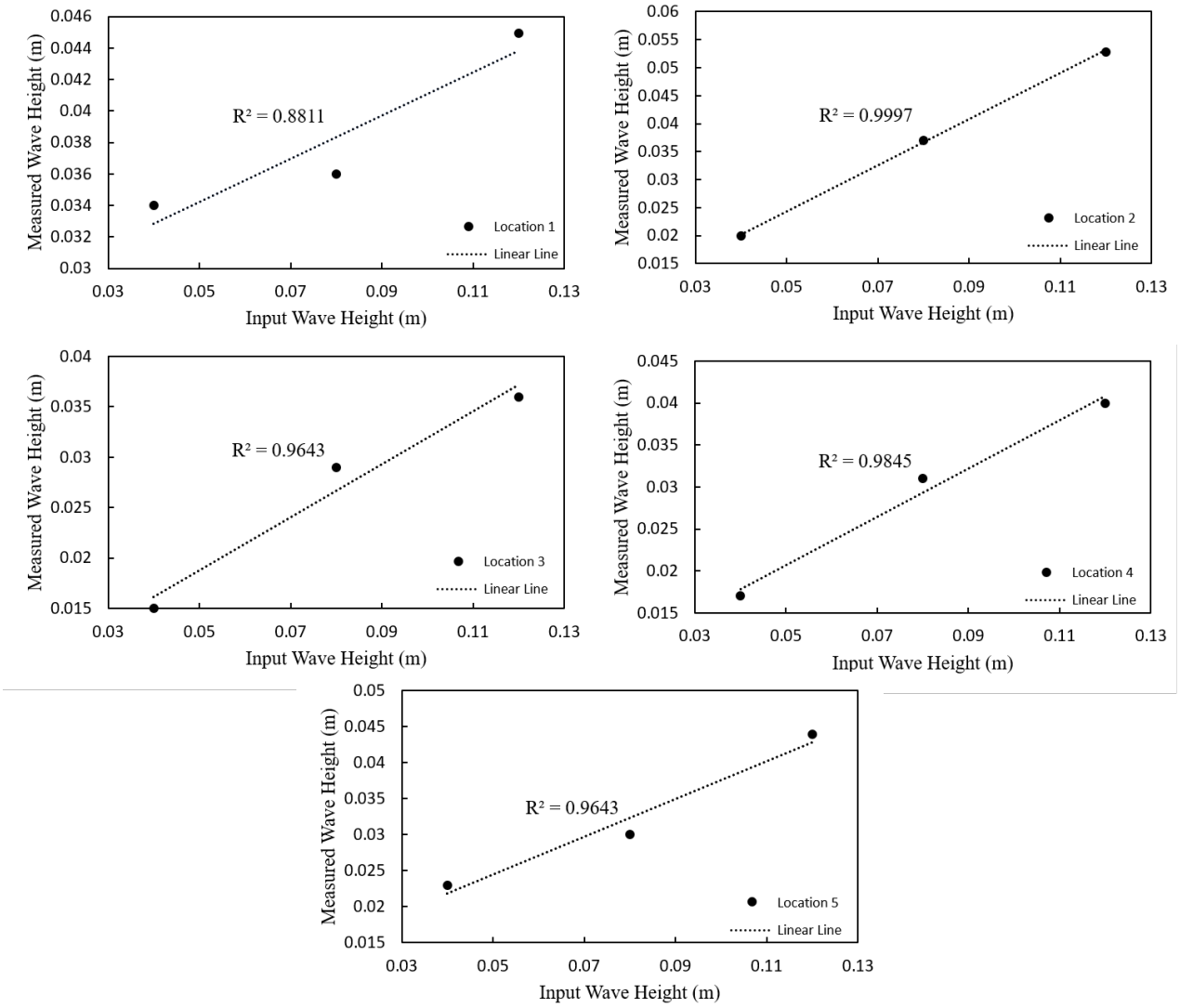

Figure 11. Incident wave calibration data by different locations

Reviewing all the calibration results in Figure 11, it is not difficult to see which location is the most accurate. By placing the sensor at location 2, the graphs have shown that the R-squared value for this location is closest to 1 compared to the other locations. The R-squared value for location 2 is 0.9997, which means that the data from this area is reliable and trustworthy. It is the site with the most accurate wave height corresponding to inputted wave height.

This experiment consisted of two types of devices, namely BBDB and PA. The BBDB model has the same basic dimensions as the numerical model but with a scale of 1:30 resulting from the F_r number, as mentioned in the previous section. This experimental model of the BBDB has the dimensions of a horizontal water column of 0.56 m length, 0.30 m height and 0.40 m width and a vertical water column of 0.4 m × 0.13 m. Transparent acrylic sheets with a thickness of 6 mm were used as the material for the production of all models. Acrylic was used because it is light and therefore easy to transport and use in wave pools for experiments. In addition, acrylic is a clear material that makes it possible to see the movement of the water in the water chamber. The movement of the water in the water chamber column is very important to study the behaviour of BBDB during the experiments. The diameter of the opening that allows air flow in both directions is 20 mm and is located at the top of the air column. This model is similar to the best performing BBDB model studied by Jalani et al. (2022). The detailed drawing and picture of the prototype of Model A can be seen in Figures 12 and 13 respectively.

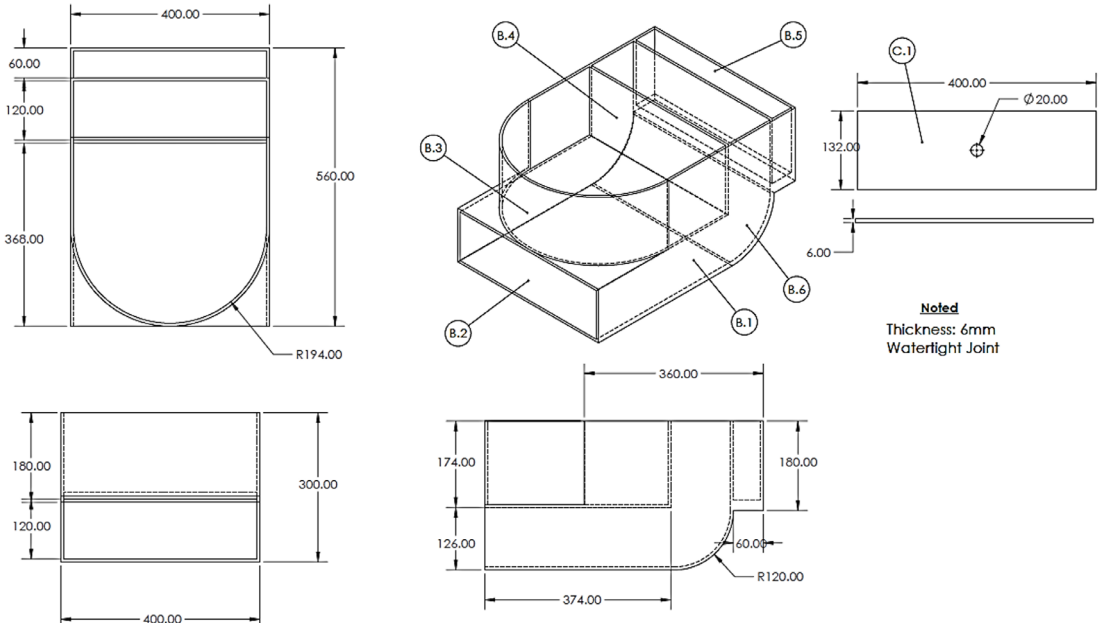

Figure 12. Detailed drawing of BBDB Model.

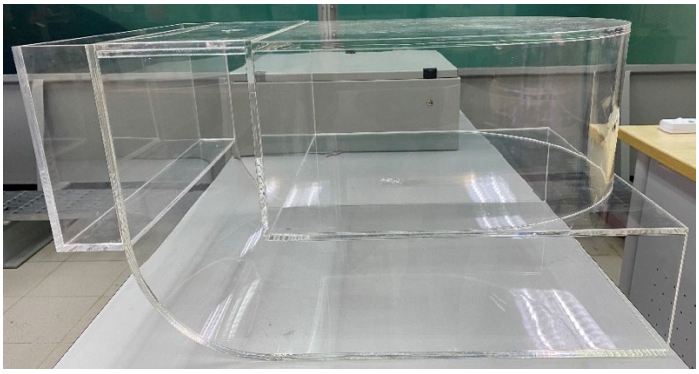

Figure 13. Prototype Picture of BBDB Model

For the PA model, commercially available polystyrene cylinder tubes with a diameter of 0.1 m and a length of 0.24 m were used to produce the experimental model from the numerical model, also on a scale of 1:30, as shown in Figure 14. Polystyrene was chosen because this material has a low density, floats more easily on the water surface and reacts quickly to changes in water level. The polystyrene was then beveled on the underside to form a 45-degree cone and smoothed with sandpaper (see Figure 15).

Figure 14. Polystyrene Picture of PA Model

Figure 15. Prototype Picture of PA Model

To integrate PA with BBDB and to reduce the time required to shift the gap length between them when performing overall experiments, BBDB and PA were connected with variations in the length of the PVC pipe stems, as shown in Figure 16. The new correlation was introduced and proved by the author (Jalani et al., 2023) and was used in this research to determine the range of length of hybrid BBDB-PA. The hybrid BBDB-PA will reach the maximum oscillation due to the maximum wave height at the peak-to-trough length, λ/2 (Saket et al., 2018). Considering the length of BBDB and the diameter of PA, the distance between BBDB and PA (L) was determined based on this equation (Jalani et al., 2023):

$$\frac{\lambda}{2} = l_{BBDB} + D_{PA} + L, \tag{2}$$

where λ is the wavelength, l_{BBDB} is the length of BBDB (parallel to the wave direction), and D_{PA} is the diameter of PA. The PVC pipe was cut based on the gap length calculated using this equation. Then, the PA was installed at the front position of BBDB, which is similar to the PA position studied by Jalani et al. (2023), proving that the front position provides higher performance for this hybrid BBDB-PA (Jalani et al., 2023). The positions of the PVC pipe between both models and the prototype of the full hybrid model are shown in Figure 17.

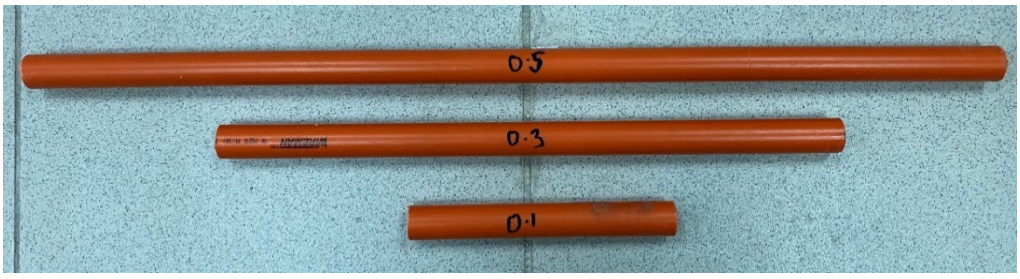

Figure 16. PVC Pipe with variation length

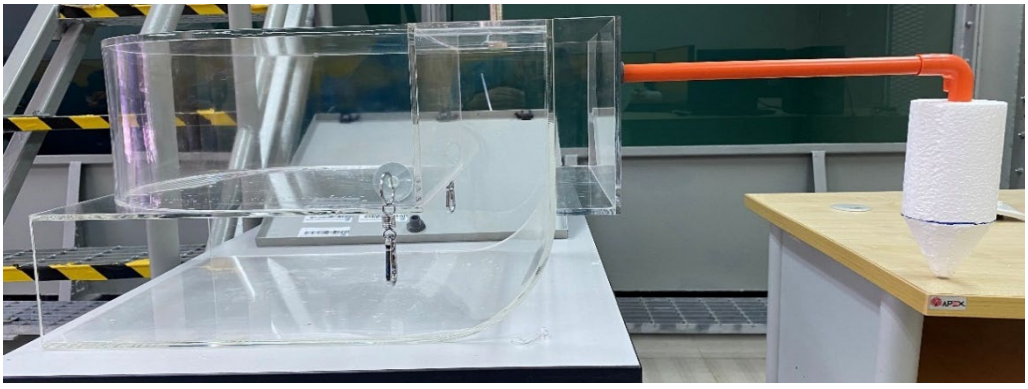

Figure 17. Prototype Picture of Full Hybrid Model

During the test phase, the hybrid BBDB-PA model was set in motion in a total of six degrees of freedom (DoF). As can be seen in Figure 18, a high-resolution camera was used to measure the lifting movements of the BBDB and PA models. This camera was able to capture the position of the BBDB and PA models, as shown in Figure 19. The optical tracking marker tape was placed on top of the PA model and in the centre of the BBDB on its port side.

Figure 18. Prototype Picture of Full Hybrid Model

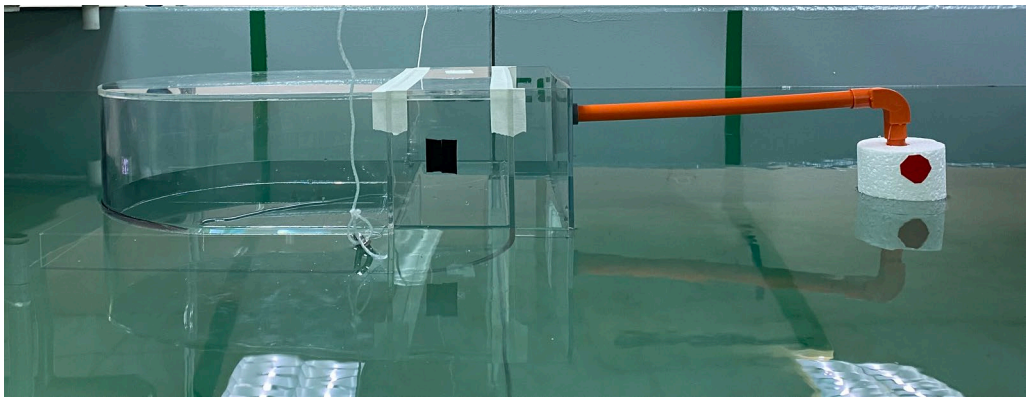

Figure 19. Prototype picture of the full hybrid model

For mooring, the BBDB was anchored in a balanced position with two mooring points located at calibrated locations as mentioned in the previous section. Each end of the mooring cable was attached to a spring anchor attached to the BBDB and another to an aluminum frame (Figure 20). The touchdown point of each mooring line was 1 m from the center of the model. The mooring rope was made of nylon with a length of 3.0 m and a rope density of 0.020 kg/m3. Two pieces of mooring rope were attached to each side of the BBDB model. Rapaka et al. (2004) investigated the effects of mooring on the motion responses of floating structures. The authors found that varying the mooring ropes from 4 to 6 reflected the same behavior and showed little difference in motions in all wave, heave and pitch modes (Rapaka et al., 2004) [25]. Considering that the effects of mooring on the motion responses of floating structures did not change significantly, the positions of the blocks were not changed in this study. At the end of each test, the position of the model and the aluminum frame was checked to ensure that they did not move through the waves during the experiment. The main function of the mooring line was to counteract the low drift force and keep the hybrid BBDB-PA in its dynamic equilibrium position. The current tests showed that the aluminum frame was strong enough to withstand the mooring forces.

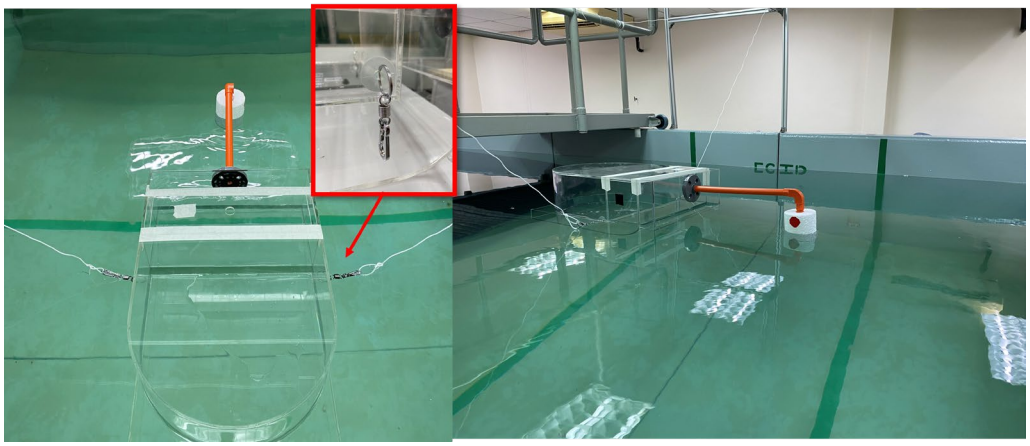

Figure 20. Complete mooring system of the experimental model

The experiments were carried out under regular wave conditions. Considering the limitations of the wave tank, the wave period was chosen to determine the tendency of all motion responses in response to different wavelengths. The primary measurement range for this experiment was determined as follows: wave period of 1 s < T < 1.5 s and slit length of 0.1 m < L < 0.5 m. The design of experiments (DoE) method was also used for this experiment. In order to more accurately predict the motion behaviour of the hybrid BBDP-PA through experimentation, two additional runs were added to each experiment for each variable. Therefore, the total number of runs for these experiments was 39 for each case. The list of selected runs generated by the statistical software is shown in Table 4.

No	Wave Height (m)	Wave Period (s)	Gap Length between BBDB and PA (m)	Experimental run number (test)
1	0.05	1.25	0.5	1
2	0.05	1.5	0.1	1
3	0.05	1.25	0.3	1
4	0.05	1.25	0.3	2
5	0.05	1.25	0.1	1
6	0.05	1.25	0.3	3
7	0.05	1.5	0.3	1
8	0.05	1.25	0.3	4
9	0.05	1	0.1	1
10	0.05	1.25	0.3	5
11	0.05	1.5	0.5	1
12	0.05	1	0.3	1
13	0.05	1	0.5	1
14	0.05	1.25	0.1	2
15	0.05	1.25	0.3	6
16	0.05	1.25	0.5	2
17	0.05	1.25	0.3	7
18	0.05	1	0.3	2
19	0.05	1.25	0.3	8
20	0.05	1.25	0.3	9
21	0.05	1.5	0.1	2
22	0.05	1	0.1	2
23	0.05	1.25	0.3	10
24	0.05	1.5	0.3	2
25	0.05	1.5	0.5	2
26	0.05	1	0.5	2
27	0.05	1.25	0.3	11
28	0.05	1.25	0.3	12

29	0.05	1.25	0.1	3
30	0.05	1.5	0.5	3
31	0.05	1	0.1	3
32	0.05	1.25	0.3	13
33	0.05	1.25	0.3	14
34	0.05	1.25	0.3	15
35	0.05	1	0.3	3
36	0.05	1.5	0.3	3
37	0.05	1.25	0.5	3
38	0.05	1.5	0.1	3
39	0.05	1	0.5	3

Table 4. Selected run for motion experiment

To determine the RAO of the floating structures, the carefully measured data from the experiments must be analyzed. In order to analyze the data measured by the devices, some steps must be carried out to derive the RAO of the movement of the structures. This method was also proposed by Alamian et al. to determine the average amplitude and period of waves and responses (Alamian et al., 2017).

To analyze the motion structure in the video, the commercially available software Tracker was used in this study. This software processes the images from a high-pixel camera to obtain the uplift data from the hybrid BBDB-PA model. The calibration of the video pixels was adjusted to ensure accuracy and synchronization between pixels and actual distance in the video. In the software, the calibration was performed by inserting the calibration stick to measure the exact distance in the project video. As shown in Figure 21, the length of the calibration rod (blue line) is 0.56 m, which is the accurate measurement of the BBDB length.

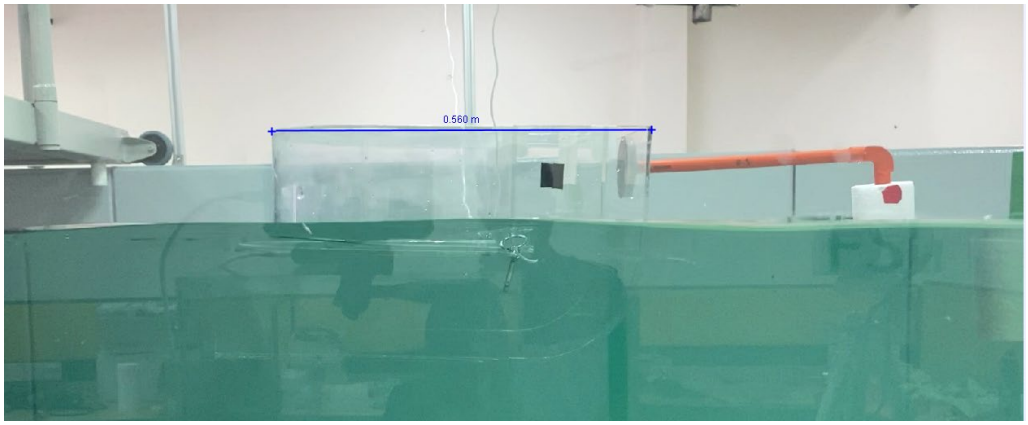

Figure 21. Tracker software calibration tool.

Once selected optical tracking markers have been assigned, the movement of the marker is automatically tracked using the software functions. The software automatically generates a time series of data based on the tracking of the assigned points on the previously prepared optical tracking marker tape. Once tracked, the data can be displayed in tabular form and in a sinoidal graph showing the uplift movement versus time plot. Figure 22 illustrates the data generated and collected by the software.

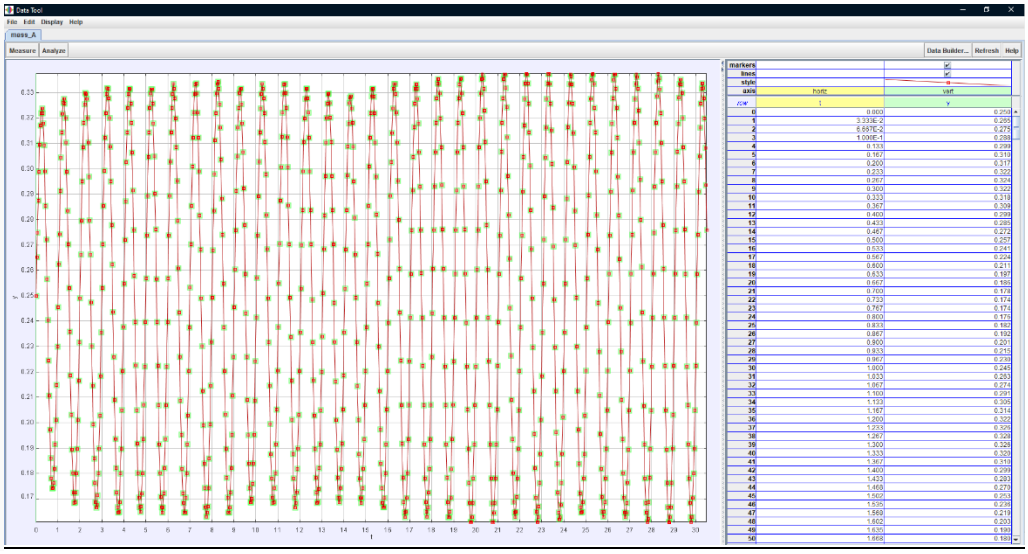

Figure 22. Tracker software collected data.

4. RESULTS AND DISCUSSION

Figure 23 depicts the contour plots and response surfaces of the uplift RAO as a function of the gap length (L) and the wave period (T) of the hybrid BBDB-PA. The contour plots show a peak in the middle region, which exhibits an initial increase followed by a subsequent decrease in both gap length and wave period. This contour plot was translated into the shape of a hill in the response surface, showing peaks in the center and troughs at the edges. This result was similar to the previous simulation result of the RAO response to the slit length. The observed phenomenon can be attributed to the resonant frequency of the model. In simple terms, the heave RAO can be directly affected by the resonant frequency of the hybrid BBDB-PA. In addition, the wave period has a great influence on the wavelength in determining the natural heave period. From the contour plot, it can be concluded that the optimal range for the gap length and wave period to maximize the heave RAO is (0.25 - 0.35 m) and (1.2 - 1.3 s), respectively.

The result of the optimization design analysis is a main effect plot for the mean heave RAO, which is shown in Figure 24. It can be observed that the wave period of 1.25 s and the gap length of 0.3 m was the best optimized value for the maximum heave RAO. This may be due to the fact that the wavelength, which is affected by the wave period, is the same as the length of the hybrid BBDB-PA, which is affected by the gap. Therefore, it can be concluded that the wave period and the gap can affect the performance of the hybrid BBDB-PA at the heave RAO.

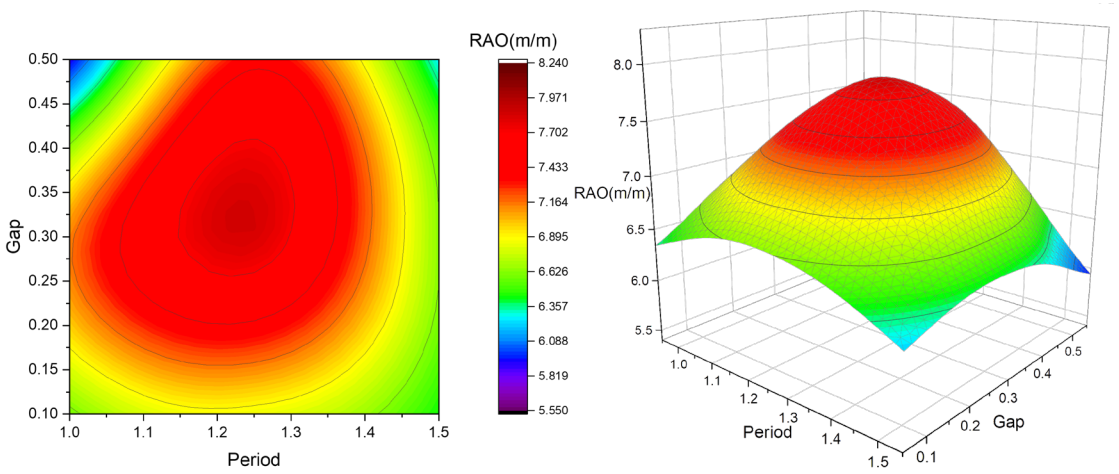

Figure 23. Response surface plots (contour (L) and 3D (R)) for RAO showing the effect of Gap and Period

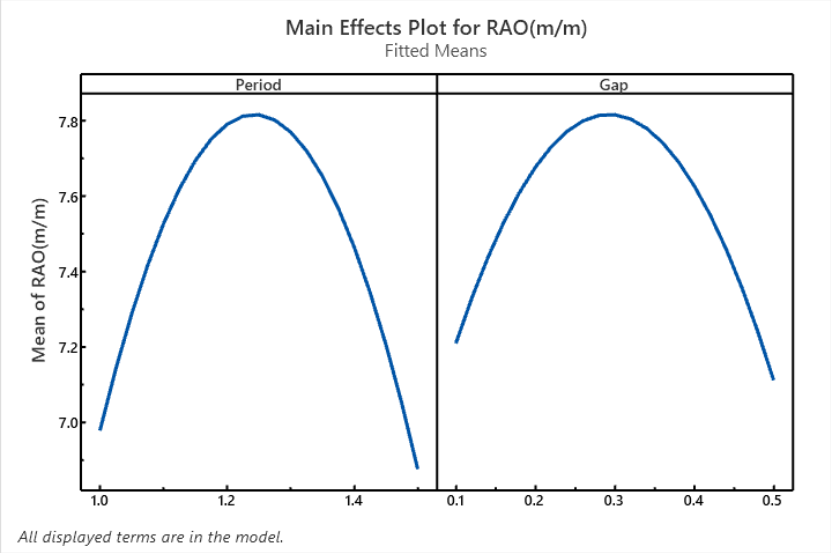

Figure 24. Main Effects plots (Period (L) and Gap (R)) for Mean of RAO

The purpose of this section was to compare the performance of the individual 1:30 scale wind turbine models for hybrid and non-hybrid forms in terms of lifting RAO. However, due to limitations in the experimental setup and movement mechanism, the experiment could not be conducted for non-hybrid PA. However, the hybrid PA was compared with the empirical value from the empirical equation studied by Jalani et al. (2023) [23]. Figure 25 shows the motion RAOs of all tested hybrid and non-hybrid models at different wave periods. The trends of the results of the present study are significant to the empirical results. However, the simulation cannot predict a slight difference in the RAO value due to the compressibility and viscosity effects of the air. Not considering the wave period parameter in the empirical equation of the previous study leads to a constant value for the empirical results. The hybrid BBDB-PA performed better by exhibiting a larger RAO value for uplift than its non-hybrid counterpart. In the hybrid form, the heave RAO value exhibited a maximum value that occurred at a time closer to 1.25 s. The occurrence of this peak can be attributed to the resonant frequency resulting from the interaction of multiple bodies. The hybrid shape has a longer contact wavelength compared to the non-hybrid shape, which is associated with a higher RAO value for the uplift. This observation is consistent with the model studied by Zheng and Zhang (2018). In addition, the introduction of the hybrid shape led to a change in the peak value of the non-hybrid BBDB, which was shifted from T=1.0 s to T=1.25 s. This change can be attributed to the adjustment of the resonant frequency of the BBDB. In addition, a hybrid configuration facilitates the extraction of energy from waves reflected by another model. The radiation wave emitted from a nearby structure is considered as an incident wave that hits the affected structure, thereby amplifying its motion. This result is consistent with the earlier study by Cheng et al. (2022), which calls the shielding effect.

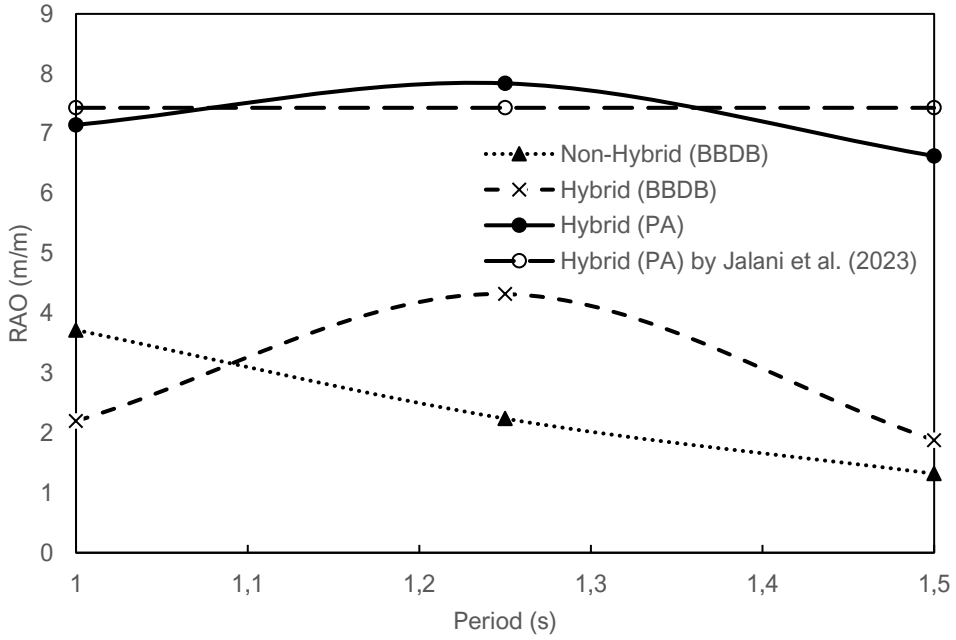

Figure 25. Heave motion RAO vs Wave Period for Hybrid and Non-Hybrid

5. CONCLUSION

The present study attempts to investigate the effects of implementing different gap length dimensions on a novel iteration of the BBDB floating OWC that incorporates a PA-OB system. This investigation focuses specifically on assessing the suitability of this hybrid system for the prevailing wave conditions in Kuantan Harbor. The aforementioned models were thoroughly tested in a 2D wave flume using a comprehensive set of frequency domain analyzes. In addition, a statistical analysis technique widely known as DOE was introduced and applied. The results of this study can be summarized as follows;

- The local sea properties were elucidated by analyzing two weeks of data collected by an Acoustic Wave and Current (AWAC) meter. These results were then extrapolated to create a simulated data set for the duration of one year. The results show a predominant wave period denoted by Tp = 3 s. In addition, an average significant height is given as Hs = 0.8 m.
- The effects of different wave periods and gap lengths on the uplift RAO of the hybrid BBDB-PA were investigated. The results obtained consist of contour and surface plots representing the state parameters. The optimal parameter was selected as T = 1.25 s and L = 0.3 m for the mini model defined by the wave characteristics of Fr Number from Kuantan Harbor. These parameters were enhanced by the Response Surface Method (RSM).
- The relationship between the gap length between PA and BBDB and the wavelength showed a direct correlation. This correlation is consistent with the theoretical expectation for the peak-to-trough length, which is the distance at which the maximum wave height is observed.
- The hybrid shape has a higher RAO value compared to the non-hybrid shape, which can be attributed to the resonant frequency resulting from the interaction of multiple bodies. The hybrid form has a longer contact wavelength compared to the non-hybrid form.
- In the context of evaluating WEC devices in a hybrid system, it is found that the PA achieves better wave energy conversion results compared to the BBDB over a majority of the wave periods tested. This phenomenon is due to the shielding effect of the PA, which effectively reduces the interaction of the wave with the BBDB under certain wave conditions. Conversely, wave reflection at the boundary between the water body and the breakwater (BBDB) enhances the oscillatory movement of the advancing waves.
- In contrast to single BBDB and PA devices, the hybrid concept is a more favorable option as it is able to achieve a high RAO and greater wave attenuation. In addition, the hybrid system enables the realization of a wider range of wave periods that can be effectively utilized.

It is important to emphasize that changing the size and length of the device may lead to an increase in construction, operation and maintenance costs as the overall parameters of the device are extended. The main focus of this research pertains to the hydrodynamics and wave power absorption of the Hybrid BBDB-PA. However, it is crucial to also consider the strength and stress analysis of the device. This evaluation exceeds the limits of current research and will be postponed to future investigations.

ACKNOWLEDGEMENTS

This study was performed under funding assistance from Akaun Amanah Industri Bekalan Elektrik (AAIBE) (UPNM/2018/AAIBE-KETTHA/TK/1/P4), Universiti Pertahanan Nasional Malaysia and Ministry of Higher Education Malaysia (FRGS/1/2020/TK0/UPNM/02/3). This study also was performed under the Cooperative Research Program of IOES, Institute of Ocean Energy, Saga University, Japan (\#22-B-04) (UPNM/2022/SAGA UNIVERSITY/TK/02).

CONFLICT OF INTEREST

The authors declared no conflicts of interest with respect to the research, authorship and publication of this article.

REFERENCES

Alamian, R., Shafaghat, R., Shadloo, M.S., Bayani, R. and Amouei, A.H. (2017) 'An empirical evaluation of the sea depth effects for various wave characteristics on the performance of a point absorber wave energy converter', Ocean Engineering, 137, pp. 13–21. Available at: https://doi.org/10.1016/j.oceaneng.2017.03.036.

Amin, M., Shah, H.H., Fareed, A.G., Khan, W.U., Chung, E., Zia, A., Farooqi, Z.U.R. and Lee, C. (2022) 'Hydrogen production through renewable and non-renewable energy processes and their impact on climate change', International Journal of Hydrogen Energy, 47(77), pp. 33112–33134. Available at: https://doi.org/10.1016/j.ijhydene.2022.07.172.

Çelik, A. and Altunkaynak, A. (2019) 'Experimental investigations on the performance of a fixed-oscillating water column type wave energy converter', Energy, 188, p. 116071. Available at: https://doi.org/10.1016/j.energy.2019.116071.

Chakrabarti, S. (1998) 'Physical model testing of floating offshore structures', Dynamic Positioning Conference, 1, pp. 1–33.

Cheng, Y., Fu, L., Dai, S., Collu, M., Cui, L., Yuan, Z. and Incecik, A. (2022) 'Experimental and numerical analysis of a hybrid WEC-breakwater system combining an oscillating water column and an oscillating buoy', Renewable and Sustainable Energy Reviews, 169, p. 112909. Available at: https://doi.org/10.1016/j.rser.2022.112909.

Chowdhury, M.S., Rahman, K.S., Selvanathan, V., Nuthammachot, N., Suklueng, M., Mostafaeipour, A., Habib, A., Akhtaruzzaman, M., Amin, N. and Techato, K. (2021) 'Current trends and prospects of tidal energy technology', Environment, Development and Sustainability, 23, pp. 8179–8194. Available at: https://doi.org/10.1007/s10668-020-01013-4.

Giannini, G., Temiz, I., Rosa-Santos, P., Shahroozi, Z., Ramos, V., Göteman, M., Engström, J., Day, S. and Taveira-Pinto, F. (2020) 'Wave energy converter power take-off system scaling and physical modelling', Journal of Marine Science and Engineering, 8(9), p. 632. Available at: https://doi.org/10.3390/jmse8090632.

Hughes, S.A. (1993) Physical models and laboratory techniques in coastal engineering. Vol. 7. Singapore: World Scientific. Available at: https://doi.org/10.1142/2154.

Isa, N.A., Baharudin, Z.A., Zainuddin, H., Sutikno, T., Zainon, M. and Zulkefle, A.A. (2021) 'Distribution of attempted leader with monsoon seasons and negative cloud-to-ground flashes in Melaka, Malaysia', Indonesian Journal of Electrical Engineering and Computer Science, 23(3), pp. 1324–1330. Available at: https://doi.org/10.11591/ijeecs.v23.i3.pp1324-1330.

ITTC (2011) Recommended procedures and guidelines: Resistance Test.

Jalani, M.A., Ismail, N.I., Saad, M.R., Samion, M.K.H., Imai, Y., Nagata, S. and Rahman, M.R.A. (2022) 'Experimental study on a bottom corner of the floating WEC', Ocean Engineering, 243, p. 110237. Available at: https://doi.org/10.1016/j.oceaneng.2021.110237.

Jalani, M.A., Saad, M.R., Abdullah, M.F., Md Naiem, M.A., Razali, M.N., Zainal Abidin, N. and Abdul Rahman, M.R. (2023) 'A statistical analysis for optimisation of a hybrid BBDB-PA in Mantanani Island, Sabah', Journal of Marine Science and Engineering, 11(2), p. 386. Available at: https://doi.org/10.3390/jmse11020386.

Jalani, M.A., Saad, M.R., Samion, M.K.H., Imai, Y., Nagata, S. and Rahman, M.R.A. (2023) 'Numerical study on a hybrid WEC of the Backward Bent Duct Buoy and Point Absorber', Ocean Engineering, 267, p. 113306. Available at: https://doi.org/10.1016/j.oceaneng.2022.113306.

Kai, L.Y., Sarip, S., Kaidi, H.M., Ardila-Rey, J.A., Samsuddin, N.M., Muhtazaruddin, M.N., Muhammad-Sukki, F. and Aziz, S.A. (2021) 'Current status and possible future applications of marine current energy devices in Malaysia: A review', IEEE Access, 9, pp. 86869–86888. Available at: https://doi.org/10.1109/ACCESS.2021.3088761.

Lavidas, G. and Blok, K. (2021) 'Shifting wave energy perceptions: The case for wave energy converter (WEC) feasibility at milder resources', Renewable Energy, 170, pp. 1143–1155. Available at: https://doi.org/10.1016/j.renene.2021.02.041.

Portillo, J.C.C., Reis, P.F., Henriques, J.C.C., Gato, L.M.C. and Falcão, A.F.O. (2019) 'Backward bent-duct buoy or frontward bent-duct buoy? Review, assessment and optimisation', Renewable and Sustainable Energy Reviews, 112, pp. 353–368. Available at: https://doi.org/10.1016/j.rser.2019.05.026.

Qiao, D., Zhi, G., Liang, H., Ning, D., Yan, J. and Li, B. (2021) 'Scaling orchestration in physical model test of oscillating buoy wave energy converter', Frontiers in Marine Science, 8, p. 627453. Available at: https://doi.org/10.3389/fmars.2021.627453.

Raihan, A. and Tuspekova, A. (2022) 'Role of economic growth, renewable energy, and technological innovation to achieve environmental sustainability in Kazakhstan', Current Research in Environmental Sustainability, 4, p. 100165. Available at: https://doi.org/10.1016/j.crsust.2022.100165.

Rapaka, E.V., Natarajan, R. and Neelamani, S. (2004) 'Experimental investigation on the dynamic response of a moored wave energy device under regular sea waves', Ocean Engineering, 31(5–6), pp. 725–743. Available at: https://doi.org/10.1016/j.oceaneng.2003.09.001.

Saket, A., Peirson, W.L., Banner, M.L. and Allis, M.J. (2018) 'On the influence of wave breaking on the height limits of two-dimensional wave groups propagating in uniform intermediate depth water', Coastal Engineering, 133, pp. 159–165. Available at: https://doi.org/10.1016/j.coastaleng.2017.12.015.

Shadman, S., Hanafiah, M.M., Chin, C.M.M., Yap, E.H. and Sakundarini, N. (2021) 'Conceptualising the sustainable energy security dimensions of Malaysia: A thematic analysis through stakeholder engagement to draw policy implications', Sustainability, 13(21), p. 12027. Available at: https://doi.org/10.3390/su132112027.

Wan, C., Yang, C., Bai, X., Bi, C., Chen, H., Li, M., Jin, Y. and Zhao, L. (2023) 'Numerical investigation on the hydrodynamics of a hybrid OWC wave energy converter combining a floating buoy', Ocean Engineering, 281, p. 114818. Available at: https://doi.org/10.1016/j.oceaneng.2023.114818.

Yang, C., Xu, T., Wan, C., Liu, H., Su, Z., Zhao, L., Chen, H. and Johanning, L. (2023) 'Numerical investigation of a dual cylindrical OWC hybrid system incorporated into a fixed caisson breakwater', Energy, 263, p. 126132. Available at: https://doi.org/10.1016/j.energy.2022.126132.

Zhang, Y., Zhao, Y., Sun, W. and Li, J. (2021) 'Ocean wave energy converters: Technical principle, device realization, and performance evaluation', Renewable and Sustainable Energy Reviews, 141, p. 110764. Available at: https://doi.org/10.1016/j.rser.2021.110764.

Zhao, X., Xue, R., Geng, J. and Göteman, M. (2021) 'Analytical investigation on the hydrodynamic performance of a multi-pontoon breakwater-WEC system', Ocean Engineering, 220, p. 108394. Available at: https://doi.org/10.1016/j.oceaneng.2020.108394.

Zhao, X.L., Ning, D.Z. and Liang, D.F. (2019) 'Experimental investigation on hydrodynamic performance of a breakwater-integrated WEC system', Ocean Engineering, 171, pp. 25–32. Available at: https://doi.org/10.1016/j.oceaneng.2018.10.036.

Zheng, S. and Zhang, Y. (2018) 'Analytical study on wave power extraction from a hybrid wave energy converter', Ocean Engineering, 165, pp. 252–263. Available at: https://doi.org/10.1016/j.oceaneng.2018.07.021.